

Thermal conductivity and electrical resistivity of solid iron at Earth's core conditions from first-principles

Junqing Xu,¹ Peng Zhang,² K. Haule,³ and R. E. Cohen^{1,4,*}

¹*Department of Earth and Environmental Sciences,
LMU Munich, Theresienstrasse 41, 80333 Munich, Germany*

²*Department of Physics, Xi'an Jiaotong University, Xi'an, Shanxi, 710049, P. R. China*

³*Department of Physics, Rutgers University, Piscataway, New Jersey 08854, USA*

⁴*Extreme Materials Initiative, Geophysical Laboratory,
Carnegie Institution for Science, Washington, DC 20015-1305, USA*

(Dated: June 23, 2022)

We compute the thermal conductivity and electrical resistivity of solid hcp Fe to pressures and temperatures of Earth's core. We find significant contributions from electron-electron scattering, usually neglected at high temperatures in transition metals. Often the Wiedemann-Franz law (1853) is used to compute thermal conductivity for electrical resistivity, but we find, consistent with earlier results (*Pourovskii et al., 2017*) that the conventional relationship is violated due to electron-electron scattering, although we disagree about iron being a simple Fermi liquid at high temperatures. We obtain thermal and electrical conductivities that are consistent with experiments considering reasonable errors. The predicted thermal conductivity is reduced from previous estimates that neglect electron-electron scattering, and suggests that the geodynamo may be sustained by thermal convection.

The thermal conductivity of iron (Fe) and its alloy at Earth's core conditions is of central importance to understand the thermal evolution of Earth's core and the energetics of the geomagnetic field [1–3]. A wide range of values for the thermal conductivity at core conditions have been predicted [3–8]. Previously, thermal conductivity of iron at extreme conditions has been obtained from the electrical resistivity by applying the Wiedemann-Franz law: $\kappa = L_0 T \sigma$, where κ and σ are the thermal and electrical conductivities, σ is the inverse of electrical resistivity ρ and L_0 is the conventional Lorenz number ($2.44 \times 10^{-8} \text{ W}\Omega\text{K}^{-2}$) [9–11]. The Wiedemann-Franz "law" has generally not been verified for any material at extreme conditions. It can be derived under approximations [12] that would not apply under the high temperature conditions of Earth's core. Direct measurements of thermal conductivity at conditions close to Earth's core conditions gave low values (e.g., $46 \text{ W m}^{-1} \text{ K}^{-1}$) [13] that would support the conventional thermal dynamo picture and are consistent with a geodynamo operating through Earth history. However, the thermal conductivity measurements and electrical resistivity measurements [11] are inconsistent, requiring extreme violations of the Wiedemann-Franz law. High values of thermal conductivity ($220 \text{ W m}^{-1} \text{ K}^{-1}$) predicted by first principles molecular dynamics (FPMD) with Kubo-Greenwood (KG) formula within density functional theory (DFT) [6] are inconsistent with thermal convection of the core, requiring a different mechanism [14, 15]. In addition to the relationship to heat transport, the electrical resistivity of iron and its alloys at Earth's core conditions is an important quantity for the geodynamo in itself, since a higher resistivity increases the dynamo dissipation.

We calculate both electron-phonon and electron-

electron contributions to electrical and thermal conductivity in solid hcp iron. We use the experimental equation of state (EOS) of Ref. [16], which agrees well with the theoretical EOS of Ref. [17] at pressures above 50 GPa. The e-ph contribution is calculated using the inelastic Boltzmann transport equation [18] and Density Functional Perturbation Theory (DFPT). "Inelastic" means considering the energy variation of electronic parameters like electron density of states at finite temperatures. The LDA exchange-correlation functional (Teter Pade parametrization) [19] is used. We also have tested the Perdew-Burke-Ernzerhof functional [20] with a pseudo potential having a smaller cutoff radius. Only 2% differences were found in transport properties. Single particle orbitals are occupied according to Fermi-Dirac statistics for each temperature. \mathbf{k} -point grids $24 \times 24 \times 16$ and \mathbf{q} -point grids $12 \times 12 \times 8$ are used. At high temperatures, the mean free path l of electron due to e-ph scattering becomes comparable to the lattice constant, so that resistivity saturation may become important [10]. We estimate such effects by applying the parallel resistor formula [21]:

$$\frac{1}{\rho} = \frac{1}{\rho_{\text{saturation}}} + \frac{1}{\rho_{\text{Boltzmann}}},$$

where $\rho_{\text{Boltzmann}}$ is calculated by Boltzmann theory. $\rho_{\text{saturation}} = \rho_{\text{Boltzmann}} l_{\text{Boltzmann}} / a$, where a is lattice constant and l is mean free path. l is the product of relaxation time and Fermi velocity. Compared with previous calculations by FPMD+KG [5, 6], our method to calculate e-ph contribution is theoretically worse in handling the inharmonic effects but our results generally agree with theirs. Our thermal conductivity results agree well with those in Ref. [5] but some worse with those in Ref. [6]. Our method seems easier to achieve good

convergence than FPMD+KG. In practice, parameters in FPMD+KG simulations, especially the cell size and number of k points grids, are difficult to be converged for high-density metal. For instance, due to the finite size, states are discrete so that low frequency part of optical electrical and thermal conductivity and their dc values will depend on the choice of the width of the broadening function.

Density Functional Theory + Dynamical Mean Field Theory (DFT+DMFT) [22, 23] is applied to study the e-e contributions in its embedded [24] and stationary [25] implementation. The Hubbard parameter U and the Hund's coupling J are 5 eV and 0.943 eV, respectively. The double counting energy E_{dc} is calculated from the fully localized limit formula $E_{dc} = U(n_{cor}^0 - 0.5) - 0.5J(n_{cor}^0 - 1)$, where n_{cor}^0 is nominal electron occupancy of the correlated atom and is set to 7. The continuous time quantum Monte Carlo (CTQMC) impurity solver [26, 27] is used to obtain self-energy on imaginary-frequency axis. To obtain the self-energy along the real-frequency axis, we use maximum entropy analytic continuation, which was compared and tested against Pade and singular value decomposition methods, giving identical results. The lattice is solved with the correlated self-energy using the all-electron LAPW (linearized augmented plane wave) WIEN2K code [28]. The DMFT results were previously reported [7], which was retracted [29] due to a factor of two error in the final resistivities due to neglect of the 2 spin channels. With self-energy on real-energy axis added to the Hamiltonian, Green's function is obtained from the eigensystem of the Hamiltonian matrix, so that transport properties can be calculated using the Kubo formula [24, 30]. The integrals are done on k-point grids $26 \times 26 \times 14$ and energy $[-10 k_B T, 10 k_B T]$ around chemical potential.

Firstly, we compare our computed isotropically averaged resistivity at $T = 2000$ K and $P = 100$ GPa with diamond anvil cell (DAC) data [11] and previous DFT results [31] (Fig. 1). The computed resistivity is anisotropic, with $\rho_a / \rho_c = 1.3$. We find that $\rho_{saturation}$ is about $160 \mu\Omega \text{ cm}$ at $V = 47.8 \text{ bohr}^3$ per atom, and increases as volume increases or pressure decreases. Our resistivities are somewhat higher than the experimental data at 100 GPa, but broadly consistent, considering the possibility of preferred orientation in the DAC experiments, temperature gradients, and the large size of the probe wires compared with the sample. At 100 GPa we also show general agreement with the FPMD results. Our calculated results along the Hugoniot agree with the shock data from the experiments (see Fig. 2) [9, 32] within the admittedly large scatter.

We compare our calculated resistivity with previous theoretical and experimental results at the core density of iron (13.04 gcm^{-3} , or an atomic volume of $47.8 \text{ atomic units} = 7.083 \text{ \AA}^3$) (Fig. 3). Our e-ph results are slightly higher but in general agreement with the FPMD results

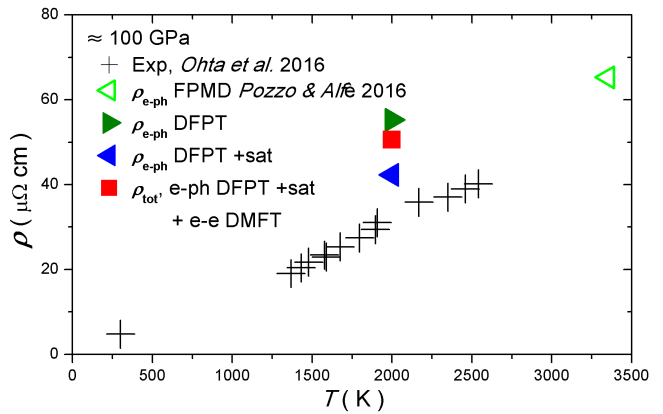


FIG. 1. Calculated resistivity at $T = 2000$ K and $P \approx 100$ GPa compared with DAC experimental data [11] and FPMD+KG results [31]. ρ_{e-ph} is the e-ph contribution of resistivity calculated by DFPT + inelastic Boltzmann theory, '+ sat' includes resistivity saturation effects for the e-ph scattering, and '+ e-e' is the e-e contribution of resistivity. ρ_{tot} is total resistivity considering both e-ph and e-e scatterings.

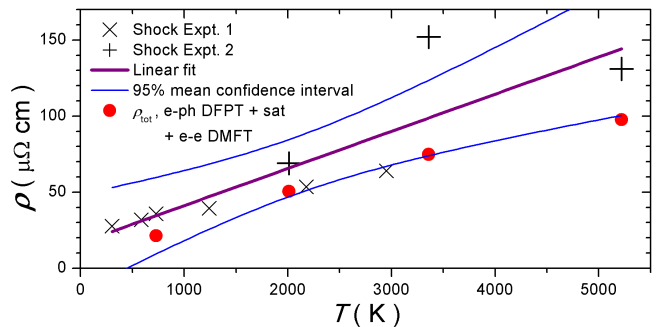


FIG. 2. Resistivity along the Hugoniot from shock data. 'x' are from Ref. [9] and '+' are from Ref. [32]. The purple line is the linear fit of shock compression data. The blue lines are the 95% mean confidence interval.

[31]. Our total resistivity is in quite poor agreement with the extrapolation values of DAC data [11] at 212 GPa, considering that at 6000 K the core density of iron corresponds to a pressure above 300 GPa. This is partly due to the increasing differences between our theoretical resistivities and the DAC experimental data at larger pressures. The use of smaller $\rho_{saturation}$ and the neglect of the e-e scattering in the temperature dependence of the resistivity in their extrapolation lead to further differences between their extrapolation at 212 GPa and our calculation. At higher temperatures e-e scattering becomes more important, and reaches about 35% of the e-ph value at Earth core conditions.

Pourovskii et al. [34] also performed DMFT transport calculations for hcp Fe at high pressures and temperatures. They found $\rho_{e-e} \propto T^2$, and claim nearly perfect Fermi liquid behavior of solid hcp Fe at all temperatures. It has been proven that the strong energy-

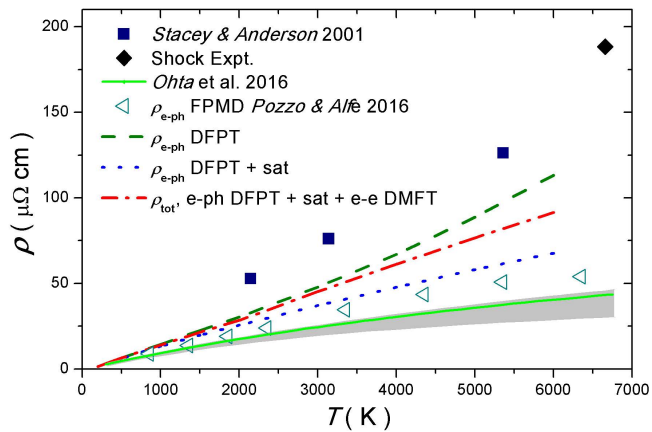


FIG. 3. Resistivity versus temperatures of hcp Fe at Earth's inner core density. The olive dash, blue dot and red dash dot lines are our theoretical results. The open triangle is FPMD results [31], where there is no e-e contribution, at a little higher density. The navy squares are extrapolations to this density using the systematics of Stacey and Anderson [33] based on the melting curve (which has no fundamental justification). The dark diamond is an interpolation to this density and an extrapolation to temperature 6658 K of previous shock compression results [9, 32]. The green line is from Ref. [11], and is the extrapolation of their experimental data.

dependence of τ_{e-e} of a Fermi liquid [35] will lead to a constant Lorenz number for e-e scattering, about $1.58 \times 10^{-8} \text{ W}\Omega\text{K}^{-2}$ [36, 37], strongly reduced from the conventional L_0 of $2.44 \times 10^{-8} \text{ W}\Omega\text{K}^{-2}$. However, our calculations do not support the statement of Fermi liquid behavior at high temperatures. At $V=47.8 \text{ bohr}^3$ per atom, both our calculated ρ_{e-e} and scattering rate at chemical potential show linear relations to temperature (Fig. S1 and S3 [30]). Moreover, the strength of the energy-dependence of τ_{e-e} decreases as temperature increases (Fig. S2 [30]). We stress here that we observe that the scattering rate is frequency dependent, as pointed out in Ref. [34], and obtain similar values of the scattering rate to theirs, however, the frequency dependence of the scattering rate has stronger effects on the thermal conductivity when properly used in the Kubo formula, as compared to simpler Fermi-liquid type approximation. We also point out that in contrast to Ref. [34], our calculation shows that hcp iron is not a simple Fermi liquid at high temperature of earths core, even when the feedback effect of the e-ph scattering on electronic correlations is neglected. As the e-ph scattering is stronger than the e-e scattering, the Fermi liquid approximation can not be expected to hold under these conditions anyway.

The Lorenz number for the e-e scattering depends not only on the energy dependence of τ_{e-e} , but also on the energy dependences of velocity and density of states. We found that Lorenz number for e-e scattering increases from about 1.4×10^{-8} to about $2.0 \times 10^{-8} \text{ W}\Omega\text{K}^{-2}$ at T

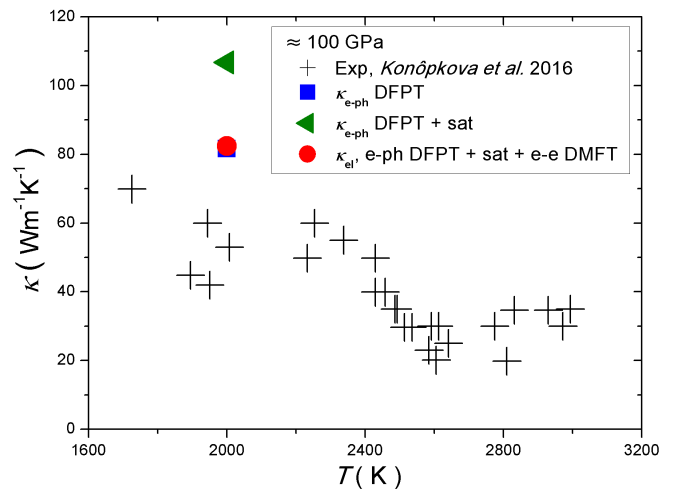


FIG. 4. Our calculated thermal conductivity of hcp Fe at about 100 GPa compared with experimental data [13]. κ_{el} is electronic part of thermal conductivity and is equal to $\kappa_{el} = [(\kappa_{e-ph} + \kappa_{sat})^{-1} + \kappa_{e-e}^{-1}]^{-1}$.

from 2000 K to 6000 K.

At this point we (and anyone) can only compute the e-ph and e-e contributions separately and add them. This is called Matthiessen's rule, which has broad experimental support but may break down at extreme conditions. Using this approximation, we compute the total electronic part of the thermal conductivity $\kappa_{el} = [(\kappa_{e-ph} + \kappa_{sat})^{-1} + \kappa_{e-e}^{-1}]^{-1}$, where κ_{e-ph} is thermal conductivity due to e-ph scattering without considering resistivity saturation effects. κ_{sat} is estimated as $L_{e-ph}T/\rho_{sat}$ and L_{e-ph} is defined as $\kappa_{e-ph}\rho_{e-ph}/T$. It is also reasonable to estimate κ_{sat} as L_0T/ρ_{sat} and κ_{sat} will be increased by at most 12 percent which will lead to only a 3.6% increase of κ_{el} .

Figure 4 shows calculated thermal conductivity of hcp Fe at 112 GPa compared with experimental data [13]. We get a somewhat higher thermal conductivity. Given the extraordinary pioneering work of both sets of experiments, we suspect that both the experimental resistivities and thermal conductivities are underestimated at core conditions, and are probably closer to our computed values.

With the theoretical thermal conductivity of liquid Fe-Si or Fe-O alloy (pure liquid iron), at the core-mantle boundary (CMB) ($T \approx 4000 \text{ K}$ and $P \approx 125 \text{ GPa}$), of about $100 (140) \text{ W m}^{-1} \text{ K}^{-1}$, the heat loss from core to mantle by conduction is estimated to be 15 terawatts (TW) [6]. The total heat from the core is estimated to 8-16 TW [39, 40], so that the conventional thermal convection geodynamo would fail. At inner core conditions our calculated electronic part of thermal conductivity of pure solid iron is $140 \text{ W m}^{-1} \text{ K}^{-1}$ (Figure 5). At 3360 K and about 140 GPa, at the uppermost outer core, we find $\kappa = 94 \text{ W m}^{-1} \text{ K}^{-1}$ [30]. Earth's outer core contains

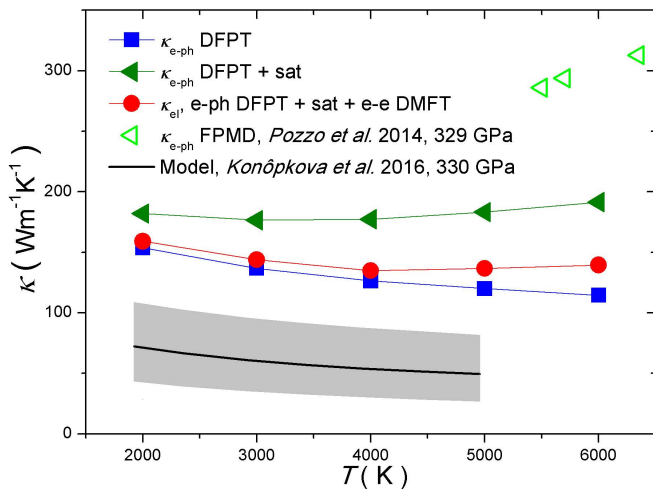


FIG. 5. Calculated thermal conductivity of solid hcp Fe at Earth’s core density, 13.04 g cm^{-3} , or atomic volume 47.8 bohr^3 . At 6000 K, the corresponding pressure is about 305 GPa. The black line is the extrapolation model at 330 GPa based on the experimental data at 112 GPa [13]. A uncertainty envelope of the model (grey) is given according to our guess that their experimental data at 2000 K and the extrapolation to pressure 330 GPa may both have errors 10-30% and thermal conductivity may decrease slower than $T^{-0.5}$ used in their model. The green open triangles are theoretical thermal conductivity at 329 GPa due to only e-ph scattering using FPMD [38], which includes saturation effects consistent with their system size and k-point sampling.

light elements of the order of 20%. Assuming light elements decrease thermal conductivity without e-e scattering contribution by 10% [6], and considering the melting may further lead to a reduction of 15% [38], the thermal conductivity would be about $75 \text{ W m}^{-1} \text{ K}^{-1}$. The corresponding heat conduction down the core adiabat will be about 9-12 TW, depending on the choice of core parameters, e.g., specific heat capacity, CMB temperature, etc. [2, 3, 6].

To determine whether a dynamo can be operated, it is necessary to know the entropy terms in Earth’s outer core region. With the reduced thermal conductivity, the adiabatic conduction entropy will be reduced to 260-420 M W K^{-1} [2, 6]. For a CMB heat flow 12 or 16 TW, if the radiogenic heating is negligible, our estimate of the entropy left would be 180-250 or 380-430 M W K^{-1} , without gravitational or compositional contribution being present. These values are not large, but may be enough for driving the geodynamo [2]. Therefore, it becomes possible again that the geodynamo is mainly sustained by thermal convection. A CMB heat flow ≥ 12 TW is some high and may lead to a young inner core age less than 1 Gyr [2].

Our theoretical thermal conductivity is 3 times higher than the extrapolation value at inner core conditions of experimental data [13]. Possible reasons are: (i) the ex-

periments may underestimate κ due to systematic errors, and may grow as temperature increases. Their extrapolation method may be not very accurate, since only the variation of thermal conductivity as a function of pressure and temperature due to e-ph scattering is considered; (ii) our estimations of saturation effects may not be accurately estimated, although they are similar to saturation effects seen in the FPMD simulations with the Kubo-Greenwood formula, and/or (iii) Matthiessen’s rule may break down. There are few studies considering the coupling of electron correlations and e-ph coupling. Using DMFT, it is found that in FeSe, e-ph coupling is enhanced due to electron correlations [41], and this has recently been verified experimentally [42].

In our current work, we have assumed that e-e scattering has the same contribution to transport properties of solid iron and liquid iron alloy. The structure difference and the existence of impurities, e.g., oxygen, may enhance or weaken the electron correlations. To study the electron correlations of liquid iron alloy, we may have to do DMFT calculations of tens of snapshots from Molecular Dynamic simulations. In the recent work in Ref. [43], they did DMFT calculations of molecular dynamics snapshots, and found that thermal disorder does not affect electron correlations.

This work was supported by the European Research Council Advanced Grant ToMCaT and by the Carnegie Institution for Science. The authors gratefully acknowledge the Gauss Centre for Supercomputing e.V. (www.gauss-centre.eu) for funding this project by providing computing time on the GCS Supercomputer SuperMUC at Leibniz Supercomputing Centre (LRZ, www.lrz.de). P. Z. acknowledges support of National Science Foundation of China (Grant 11604255).

* rcohen@carnegiescience.edu

- [1] S. Labrosse, *Physics of the Earth and Planetary Interiors* **140**, 127 (2003).
- [2] F. Nimmo, *Treatise on geophysics: Energetics of the Core* (Elsevier, 2015).
- [3] F. Stacey and D. Loper, *Physics of the Earth and Planetary Interiors* **161**, 13 (2007).
- [4] X. Sha and R. E. Cohen, *Journal of Physics: Condensed Matter* **23**, 075401 (2011).
- [5] N. de Koker, G. Steinle-Neumann, and V. Vlček, *Proceedings of the National Academy of Sciences* **109**, 4070 (2012).
- [6] M. Pozzo, C. Davies, D. Gubbins, and D. Alfe, *Nature* **485**, 355 (2012).
- [7] P. Zhang, R. Cohen, and K. Haule, *Nature* **517**, 605 (2015).
- [8] R. A. Secco, *Physics of the Earth and Planetary Interiors* **265**, 23 (2017).
- [9] R. Keeler and A. Mitchell, *Solid State Communications* **7**, 271 (1969).
- [10] H. Gomi, K. Ohta, K. Hirose, S. Labrosse, R. Caracas,

- M. J. Verstraete, and J. W. Hernlund, *Physics of the Earth and Planetary Interiors* **224**, 88 (2013).
- [11] K. Ohta, Y. Kuwayama, K. Hirose, K. Shimizu, and Y. Ohishi, *Nature* **534**, 95 (2016).
- [12] M. Jonson and G. D. Mahan, *Physical Review B* **21**, 4223 (1980).
- [13] Z. Konôpková, R. S. McWilliams, N. Gómez-Pérez, and A. F. Goncharov, *Nature* **534**, 99 (2016).
- [14] J. G. O’rourke and D. J. Stevenson, *Nature* **529**, 387 (2016).
- [15] J. Badro, J. Siebert, and F. Nimmo, *Nature* **536**, 326 (2016).
- [16] A. Dewaele, P. Loubeyre, F. Occelli, M. Mezouar, P. I. Dorogokupets, and M. Torrent, *Physical Review Letters* **97**, 215504 (2006).
- [17] X. Sha and R. E. Cohen, *Physical Review B* **81**, 094105 (2010).
- [18] P. Allen, *Physical Review B* **17**, 3725 (1978).
- [19] S. Goedecker, M. Teter, and J. Hutter, *Physical Review B* **54**, 1703 (1996).
- [20] J. P. Perdew, K. Burke, and M. Ernzerhof, *Physical review letters* **77**, 3865 (1996).
- [21] H. Wiesmann, M. Gurvitch, H. Lutz, A. Ghosh, B. Schwarz, M. Strongin, P. Allen, and J. Halley, *Physical Review Letters* **38**, 782 (1977).
- [22] A. Georges, G. Kotliar, W. Krauth, and M. J. Rozenberg, *Reviews of Modern Physics* **68**, 13 (1996).
- [23] G. Kotliar, S. Y. Savrasov, K. Haule, V. S. Oudovenko, O. Parcollet, and C. Marianetti, *Reviews of Modern Physics* **78**, 865 (2006).
- [24] K. Haule, C.-H. Yee, and K. Kim, *Physical Review B* **81**, 195107 (2010).
- [25] K. Haule and T. Birol, *Physical review letters* **115**, 256402 (2015).
- [26] K. Haule, *Physical Review B* **75**, 155113 (2007).
- [27] E. Gull, A. J. Millis, A. I. Lichtenstein, A. N. Rubtsov, M. Troyer, and P. Werner, *Reviews of Modern Physics* **83**, 349 (2011).
- [28] P. Blaha, K. Schwarz, G. Madsen, D. Kvasnicka, and J. Luitz, An augmented plane wave+ local orbitals program for calculating crystal properties (2001).
- [29] P. Zhang, R. Cohen, and K. Haule, “Retraction: Effects of electron correlations on transport properties of iron at earths core conditions,” (2016).
- [30] See Supplemental Material for more theoretical details and more detailed theoretical results.
- [31] M. Pozzo and D. Alfè, *SpringerPlus* **5**, 256 (2016).
- [32] Y. Bi, H. Tan, and F. Jing, *Journal of Physics: Condensed Matter* **14**, 10849 (2002).
- [33] F. D. Stacey and O. L. Anderson, *Physics of the Earth and Planetary Interiors* **124**, 153 (2001).
- [34] L. Pourovskii, J. Mravlje, A. Georges, S. Simak, and I. Abrikosov, *New Journal of Physics* (2017).
- [35] P. Nozières and D. Pines, *Theory of quantum liquids* (Westview Press, 1999).
- [36] C. Herring, *Physical Review Letters* **19**, 167 (1967).
- [37] C. Herring, *Physical Review Letters* **19**, 684 (1967).
- [38] M. Pozzo, C. Davies, D. Gubbins, and D. Alfè, *Earth and Planetary Science Letters* **393**, 159 (2014).
- [39] T. Lay, J. Hernlund, and B. A. Buffett, *Nature geoscience* **1**, 25 (2008).
- [40] B. Wu, P. Driscoll, and P. Olson, *Journal of Geophysical Research: Solid Earth* **116** (2011).
- [41] S. Mandal, R. E. Cohen, and K. Haule, *Physical Review B* **89**, 220502 (2014).
- [42] S. Gerber, S.-L. Yang, D. Zhu, H. Soifer, J. Sobota, S. Rebec, J. Lee, T. Jia, B. Moritz, C. Jia, *et al.*, *Science* **357**, 71 (2017).
- [43] A. Hausoel, M. Karolak, E. Şaştoğlu, A. Lichtenstein, K. Held, A. Katanin, A. Toschi, and G. Sangiovanni, *Nature Communications* **8** (2017).

Thermal conductivity and electrical resistivity of solid iron at Earth's core conditions from first-principles - Supplemental Material

Junqing Xu,¹ Peng Zhang,² K. Haule,³ and R. E. Cohen^{1,4,*}

¹*Department of Earth and Environmental Sciences,
LMU Munich, Theresienstrasse 41, 80333 Munich, Germany*

²*Department of Physics, Xi'an Jiaotong University, Xi'an, Shanxi, 710049, P. R. China*

³*Department of Physics, Rutgers University, Piscataway, New Jersey 08854, USA*

⁴*Extreme Materials Initiative, Geophysical Laboratory,
Carnegie Institution for Science, Washington, DC 20015-1305, USA*

(Dated: June 23, 2022)

TRANSPORT CALCULATION USING DMFT

Neglecting vertex correlations, dc electrical resistivity ρ_{e-e} and thermal conductivity κ_{e-e} can be computed using Kubo-Greenwood formula:

$$L_{ij} = (-1)^{i+j} \frac{\pi e^2}{V} \sum_k \int d\varepsilon \left(-\frac{df}{d\varepsilon}\right) \text{Tr}[\rho_k(\varepsilon) v_k \rho_k(\varepsilon) v_k] \varepsilon^{i+j-2},$$

$$\rho_{e-e} = \frac{1}{L_{11}},$$

$$\kappa_{e-e} = \frac{1}{e^2 T} \left(L_{22} - \frac{L_{12}^2}{L_{11}} \right),$$

where f is Fermi-Dirac statistics, v is velocity and ρ_k is spectral function on wave vector k and is related to Green's function $G(\varepsilon)$ by $\rho_k = (G^\dagger - G)/(2\pi i)$. By solving the complex eigenvalue problems $HA^R = EA^R$ and $A^L H = EA^L$, where H is the Hamiltonian with added self-energy along real-energy axis, $\Sigma(\varepsilon)$, we obtain the eigenvalue E and the eigenvectors A^R and A^L , so that $G(\varepsilon) = A^R \mathbf{1}/(\varepsilon - E) A^L$. Compared with the formulas of

Ref. [Haule *et al.*, 2010], we go beyond the approximate form of $\Sigma(\varepsilon) \approx \Sigma(0) + (1 - Z^{-1})\varepsilon - i\varepsilon^2 B$ and use the full energy dependence of the self-energy, as obtained by analytic continuation.

ELECTRON-ELECTRON SCATTERING

In Fig. S1-S3, we show scattering rates, relaxation times and resistivity due to electron-electron scattering.

COMPARISONS WITH PREVIOUS WORK

In Table S1-S6, our theoretical results of electrical resistivity and thermal conductivity are compared with other theoretical results, experimental data and results of models based on experimental data, around three kinds of conditions - about 100 GPa and 2000 K, Core-Mantle Boundary conditions and Inner Core Boundary conditions.

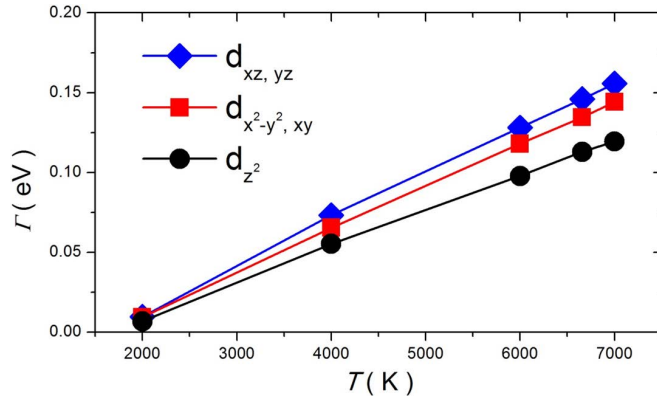


FIG. S1. Orbitally resolved scattering rate of hcp due to electron-electron scattering at atomic volume 47.8 bohr^3 .

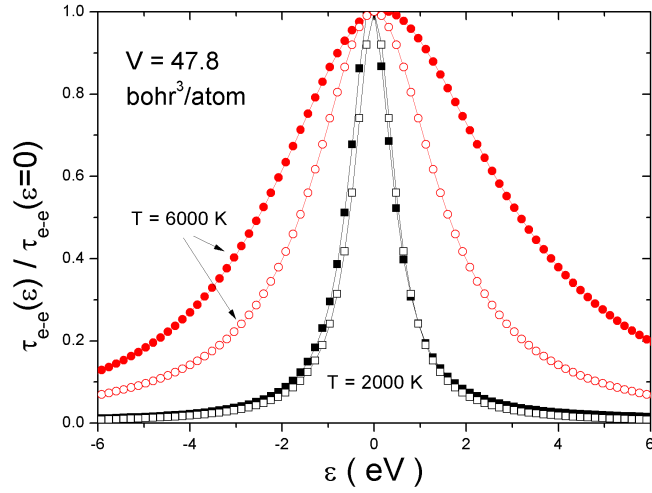


FIG. S2. Energy-dependent part of the relaxation time due to electron-electron scattering. The filled squares and circles are calculated from self-energy data given by Dynamical Mean Field Theory using $\tau(\varepsilon) = \hbar / (-2\text{Im}\Sigma(\varepsilon))$, at $V = 47.8 \text{ bohr}^3 / \text{atom}$ and $T = 2000 \text{ K}$ and 6000 K , respectively. The open squares and circles are for a Fermi liquid, which gives energy-dependent part $1/[1 + \varepsilon^2/(\pi k_B T)^2]$, at the same conditions. The relation times at chemical potential are 28.5 and 2.35 fs at $T = 2000 \text{ K}$ and 6000 K , respectively.

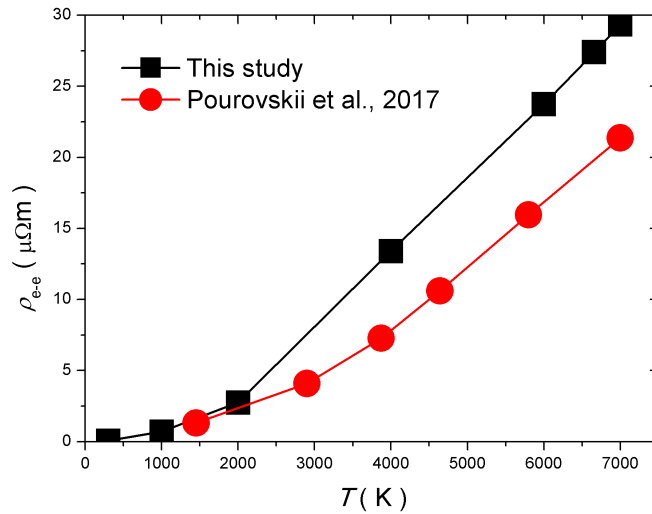


FIG. S3. Our calculated ρ_{e-e} compared with those calculated by *Pourovskii et al.*, 2017 at atomic volume 47.8 bohr^3 .

TABLE S1. Electrical resistivity at about 100 GPa and 2000 K. Our DMFT+DFPT results used the experimental equation of state by *Dewaele et al.*. All FPMD results used their own theoretical equations of state.

System	P(GPa)	V(bohr ³ /atom)	T(K)	$\rho_{e-ph}(\mu\Omega \text{ m})$	$\rho_{e-e}(\mu\Omega \text{ m})$	$\rho(\mu\Omega \text{ m})$	Type and Source
Solid Fe	110		2180			53.5	Shock Exp., <i>Keeler et al.</i>
Solid Fe	106		2000			31.1	DAC Exp., <i>Ohta et al.</i>
Solid Fe	101		2010			37.6	Model, <i>Gomi et al.</i>
Liquid Fe	122	55.9	2000	65.3			FPMD, <i>deKoker et al.</i>
Solid Fe	73	60.4	2350	52.7			FPMD, <i>deKoker et al.</i>
Solid Fe	102	57.9	2000	42.3	8.3	50.5	DFPT+DMFT, this study

TABLE S2. Thermal conductivity at about 100 GPa and 2000 K.

System	P(GPa)	V(bohr ³ /atom)	T(K)	$\kappa_{e-ph}(\text{W/m/K})$	$\kappa_{e-e}(\text{W/m/K})$	$\kappa(\text{W/m/K})$	Type and Source
Solid Fe	112		1700-2300			41.9-69.9	DAC Exp., <i>Konôpková et al.</i>
Solid Fe	112		2000			42.0	Model, <i>Konôpková et al.</i>
Liquid Fe	122	55.9	2000	82.7			FPMD, <i>deKoker et al.</i>
Solid Fe	102	57.9	2000	107	362	82.4	DFPT+DMFT, this study

TABLE S3. Electrical resistivity at Core-Mantle Boundary conditions.

System	P(GPa)	V(bohr ³ /atom)	T(K)	$\rho_{e-ph}(\mu\Omega \text{ m})$	$\rho_{e-e}(\mu\Omega \text{ m})$	$\rho(\mu\Omega \text{ m})$	Type and Source
Solid Fe	140		2950			64.1	Shock Exp., <i>Keeler et al.</i>
Solid Fe	146		2540			40.2	DAC Exp., <i>Ohta et al.</i>
Solid Fe	135		3750			53.7	Model, <i>Gomi et al.</i>
Liquid Fe	133	55.9	3000	65.4			FPMD, <i>deKoker et al.</i>
Liquid Fe	151	55.9	4000	67.9			FPMD, <i>deKoker et al.</i>
Liquid Fe ₃ Si	136	51.9	3000	102			FPMD, <i>deKoker et al.</i>
Liquid Fe	124	59.5	4630	74.7			FPMD, <i>Pozzo et al.</i>
Fe ₇₉ Si ₈ O ₁₃	134	63.3	4112	90.5			FPMD, <i>Pozzo et al.</i>
Solid Fe	146	55.1	3360	49.8	16.4	66.2	DFPT+DMFT, this study

TABLE S4. Thermal conductivity at Core-Mantle Boundary conditions.

System	P(GPa)	V(bohr ³ /atom)	T(K)	$\kappa_{e-ph}(\text{W/m/K})$	$\kappa_{e-e}(\text{W/m/K})$	$\kappa(\text{W/m/K})$	Type and Source
Solid Fe	112		2700-3000			19.8-34.6	DAC Exp., <i>Konôpková et al.</i>
Solid Fe	136		3800-4800			33±7	Model, <i>Konôpková et al.</i>
Liquid Fe	133	55.9	3000	110			FPMD, <i>deKoker et al.</i>
Liquid Fe	151	55.9	4000	133			FPMD, <i>deKoker et al.</i>
Liquid Fe ₃ Si	136	51.9	3000	75.3			FPMD, <i>deKoker et al.</i>
Liquid Fe	124	59.5	4630	154			FPMD, <i>Pozzo et al.</i>
Fe ₇₉ Si ₈ O ₁₃	134	63.3	4112	99			FPMD, <i>Pozzo et al.</i>
Solid Fe	146	55.1	3360	124	397	94.4	DFPT+DMFT, this study

TABLE S5. Electrical resistivity at Inner Core Boundary conditions. P L, *Pourovskii et al.*.

System	P(GPa)	V(bohr ³ /atom)	T(K)	$\rho_{e-ph}(\mu\Omega\text{ m})$	$\rho_{e-e}(\mu\Omega\text{ m})$	$\rho(\mu\Omega\text{ m})$	Type and Source
Solid Fe	330		4971			43.1	Model, <i>Gomi et al.</i>
Liquid Fe	327	47.9	6000	62.0			FPMD, <i>deKoker et al.</i>
Fe ₃ Si	318	47.9	6000	91.8			FPMD, <i>deKoker et al.</i>
Liquid Fe	339	47.6	6420	64.1			FPMD, <i>Pozzo et al.</i>
Liquid Fe ₇₉ Si ₈ O ₁₃	328	52.0	5500	80.5			FPMD, <i>Pozzo et al.</i>
Solid Fe	365	46.2	6350	54.0			FPMD, <i>Pozzo et al.</i>
Solid Fe ₇₉ Si ₈ O ₁₃	329		5500	64.3			FPMD, <i>Pozzo et al.</i>
Solid Fe	305	47.8	6000	67.8	23.8	91.5	DFPT+DMFT, this study
Solid Fe		47.8	6000		16.0		DFPT+DMFT, P L

TABLE S6. Thermal conductivity at Inner Core Boundary conditions.

System	P(GPa)	V(bohr ³ /atom)	T(K)	$\kappa_{e-ph}(\text{W/m/K})$	$\kappa_{e-e}(\text{W/m/K})$	$\kappa(\text{W/m/K})$	Type and Source
Solid Fe	330		5600-6500			46±9	Model, <i>Konôpková et al.</i>
Liquid Fe	327	47.9	6000	215			FPMD, <i>deKoker et al.</i>
Liquid Fe ₃ Si	318	47.9	6000	155			FPMD, <i>deKoker et al.</i>
Liquid Fe	328	48.3	6350	246			FPMD, <i>Pozzo et al.</i>
Liquid Fe ₇₉ Si ₈ O ₁₃	328	52.0	5500	148			FPMD, <i>Pozzo et al.</i>
Solid Fe	329		6350	313			FPMD, <i>Pozzo et al.</i>
Solid Fe ₇₉ Si ₈ O ₁₃	329		5500	232			FPMD, <i>Pozzo et al.</i>
Solid Fe	305	47.8	6000	192	514	140	DFPT+DMFT, this study
Solid Fe		47.8	6000		542		DFPT+DMFT, P L